



[ICP2020]

Structural, dielectric, ferroelectric and electrical properties of lead-free $\text{Ba}_{0.9}\text{Sr}_{0.1}\text{Ti}_{0.9}\text{Sn}_{0.1}\text{O}_3$ ceramic prepared by sol-gel method.

S. Khardazi^{a*}, H. Zaitouni^a, B. Asbani^b, D. Mezzane^{a,b}, M. Amjoud^a, E. Choukri^a, S. Terenchuk^c, A. Erramli^a, Y. Gagou^b

^a IMED-Lab, Cadi Ayyad University, Marrakesh, 40000, Morocco

^b LPMC, University of Picardy Jules Verne, Amiens, 80039, France

^c Kiev National University of Construction and Architecture, Faculty of Automation and Information Technologies, Department of Information Design Technologies and Applied Mathematics, Vozdukhoflotsky Avenue, 31, 03037, Kiev, Ukraine

Abstract

Lead-free $\text{Ba}_{0.9}\text{Sr}_{0.1}\text{Ti}_{0.9}\text{Sn}_{0.1}\text{O}_3$ (BSTSn) ceramic was prepared by the sol-gel method. X-ray diffraction measurement at room temperature reveals the single-phase formation with tetragonal structure refined in the P4mm space group. Raman spectroscopy analysis at room temperature was used to confirm the structure of BSTSn ceramic sintered at 1420°C during 5h. The dielectric measurements were examined in the temperature range [-90 – 250°C] and the frequency range of [100Hz – 1MHz]. The maximum dielectric constant was found to be ~5484 (1kHz) at room temperature. The diffuse phase transition characteristic at 1kHz was ascribed by the modified Curie-Weiss law. Macroscopic polarization – field (P – E) hysteresis loops recorded at room temperature (RT) confirm the ferroelectric nature of BSTSn ceramic. Impedance spectroscopy analysis of BSTSn sample in the temperature range 300 – 380°C reveals the presence of two relaxation contributions originated from grains and grain boundaries. Activation energies of grain and grain boundaries resistances were deduced in order to determine the conduction mechanism of the studied sample.

Keywords: dielectric; lead-free ceramic; sol-gel; ferroelectric; impedance spectroscopy.

* Corresponding author. Tel.: +212608219671.
E-mail address: khardazzisaid@gmail.com

1. Introduction

During the past few decades, ferroelectric materials with perovskite structure have attracted much attention in several studies [1,2]. Especially, those exhibit large permittivity and piezoelectricity are extensively used in numerous devices, such as capacitors, piezoelectric sensors, and actuators [3]. Lead zirconate-titanate [Pb(Zr,Ti)O₃ (PZT)] present excellent dielectric, ferroelectric and piezoelectric properties [4]. This property makes them very suitable for various applications in electronic devices such as piezoelectric actuators, capacitors, sensors, etc [5]. This kind of material is limited due to the environmental impact induced by the toxicity nature of lead [4]. Barium titanate (BT) is an interesting alternative to lead-based materials due to its physical properties for developing environment-friendly materials [6, 7]. Numerous studies have been conducted to modify the BT system to enhance its dielectric and ferroelectric properties, versatility and to extend the domain of its application and functionality, including the electrocaloric properties and the energy storage capacities [8–12]. Among this family, we found Barium Strontium Titanate Ba_{1-x}Sr_xTiO₃ (BST), which is formed by the substitution of Ba²⁺ by Sr²⁺ in the A-site of BT lattice. BST system has drawn ever increasing interest, because of its applications in dynamic random-access memory, tunable microwave devices, piezoelectric transducers and multilayer ceramic capacitors [1, 13–18]. Furthermore, it has a high dielectric constant, greater polarization, and a high dielectric breakdown strength, making BST ideal for high energy storage capacities. On the other hand, we found Barium Stannate Titanate (BSTSn) designed by the substitution of Ti⁴⁺ by Sn⁴⁺ in the BT perovskite structure. Because the Curie temperature of BSTSn system could be widely shifted by changing the wt% of tin content, this solid solution can be used in various applications such as microwave phase shifter, actuator and capacitor [6, 19–21]. At present, few works have investigated the effect of simultaneous substitution of Sr²⁺ and Sn⁴⁺ in the A and B-sites of BT lattice, respectively [22, 23]. To synthesize this type of perovskite materials, various methods were employed such as solid-state technique, semi-wet method and sol-gel method [23–27]. Compared to conventional methods, the sol-gel route offers many advantages including simplicity, high control of stoichiometric composition of the phase composition, lower processing temperature and produce fine particles sizes of the powder. Moreover, the powders derived from sol-gel process are advantageous to the homogenous distribution of the composition and the microstructure, dense and better characteristics of ceramics [28, 29].

In this research work, Ba_{0.9}Sr_{0.1}Ti_{0.9}Sn_{0.1}O₃ bulk ceramics (abbreviated BSTSn) were prepared for the first time using the sol-gel method and their structure, microstructure, dielectric, ferroelectric and electric properties were investigated.

2. Experimental procedure

The Ba_{0.9}Sr_{0.1}Ti_{0.9}Sn_{0.1}O₃ (BSTSn) ceramic was prepared by the sol-gel method as described in the chart below (Fig. 1). High purity of barium acetate Ba(CH₃COO)₂, strontium acetate Sr(CH₃COO)₂·1/2H₂O, tin chloride dehydrate SnCl₂·2H₂O, and Titanium Isopropoxide (C₁₂H₂₈O₄Ti) were weighed according to stoichiometric ratios (Table 1). Acetic acid CH₃CH₂OOH and 2-methoxyethanol (C₃H₈O₂) were used as solvent agents. Stoichiometric quantities of barium acetate and strontium acetate were mixed and dissolved in acetic acid. Appropriate amounts of tin chloride dehydrate and Titanium Isopropoxide were mixed with 2-methoxyethanol under stirring for 1h. The pH~7 of the solution was adjusted by adding a Required quantity of Ammonia leading to a transparent sol. The obtained solution was heated to 80°C for 1h in the hot air oven, leading to white gel. The dried powder was calcined for 5h at 1000°C and pressed into disks using the uniaxial hydraulic press. The resulting pellets were then sintered at an optimized temperature of 1420 °C for 5h. It is interesting to note that the sintering conditions used in the present study were taken based on the density measurements using Archimedes method.

The X-ray diffraction (XRD) pattern was registered at room temperature using the Panalytical X-Pert Pro under Cu-K α radiation with $\lambda \sim 1.540598$ Å. The grain morphology of the sintered ceramic was observed by using the TESCAN VEGA3 Scanning Electron Microscope (SEM). The dielectric measurements were measured in the frequency range 100 Hz – 1 MHz and temperature interval from -90 °C to 250 °C by the Solartron Impedance Analyzer SI-1260. Room temperature polarization versus electric field (P-E) hysteresis loops were performed using a ferroelectric test system (PolyK Technologies State College, PA, USA) at 200Hz.

Table 1. Masses of raw materials used to prepare Ba_{0.9}Sr_{0.1}Ti_{0.9}Sn_{0.1}O₃ ceramics.

Mass of raw material/g			
Ba(CH ₃ COO) ₂	Sr(CH ₃ COO) ₂ ·1/2H ₂ O	SnCl ₂ ·2H ₂ O	C ₁₂ H ₂₈ O ₄ Ti
5.1763	0.4632	0.5081	5.7600

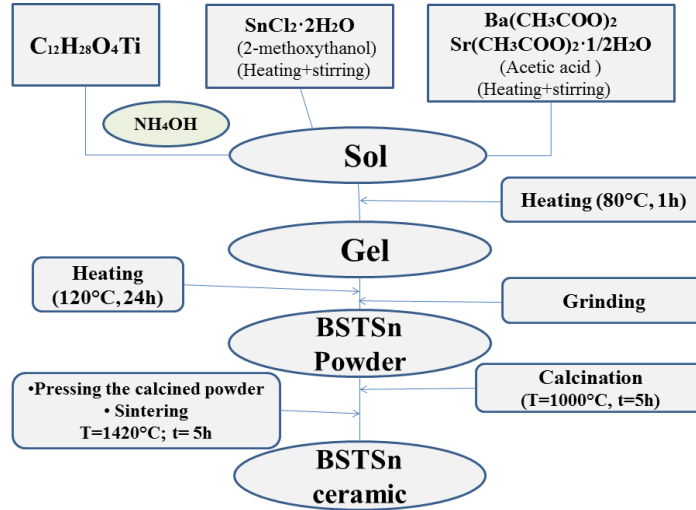


Fig. 1. Flow chart of the preparation of BSTSn ceramics by sol-gel method.

3. Results and discussion

3.1. X-ray diffractions

Room temperature X-ray diffraction patterns of BSTSn powder calcined at 1000°C for 5h is shown in Fig. 2. The sample shows a pure perovskite phase without any traces of impurities. The crystal structure of BSTSn ceramic was successfully refined in the tetragonal symmetry of the P4mm space group (by using full-prof software), suggesting the successful diffuseness of Sr and Sn into BT lattice to form a solid solution. By analyzing the shape of XRD lines, we have determined the average crystallite size of BSTSn powder using Debye Scherrer's formula [30]:

$$D = \frac{k\lambda}{\beta \cos\theta}, \quad (1)$$

where k is the Scherrer constant (generally taken as 0.9), λ is the wavelength of CuK α radiation, β is the full width at half maximum (FWHM) of the broadened diffraction peaks and θ is the measured angle. From the calculations, the average crystallites size of BSTSn powder was found to be around 45 nm. Other structural parameters such as lattice parameters and atomic positions are listed in Table 2.

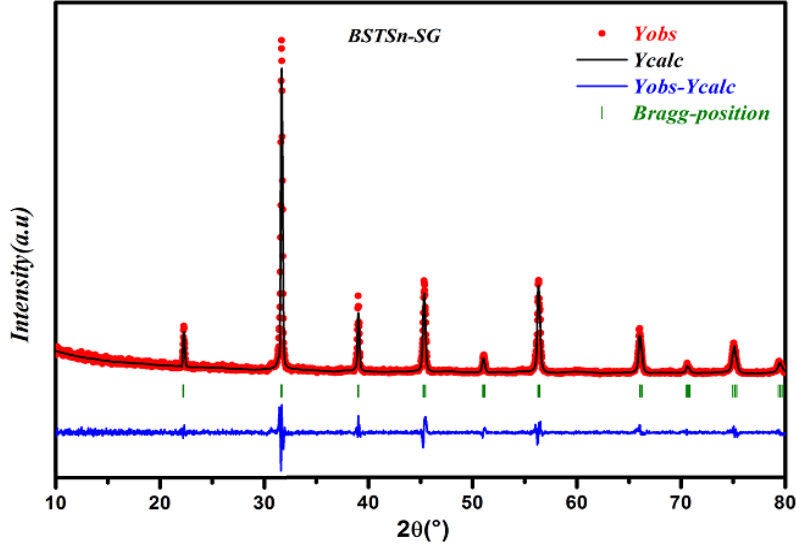


Fig. 2. X-ray diffraction patterns of $\text{Ba}_{0.9}\text{Sr}_{0.1}\text{Ti}_{0.9}\text{Sn}_{0.1}\text{O}_3$ powder calcined at $1000^\circ\text{C}/5\text{h}$.

Table 2. Structural details of BSTSn sample gathered from Rietveld refinement.

Lattice parameter(\AA)	Angle($^\circ$)	Space group	Atomic position(x, y, z)			χ^2	
a = 4.0029	$\alpha = \beta = \gamma = 90$	P4mm	Ba/Sr	0.00000	0.00000	-0.03855	1.34
b = 4.0029			Ti/Sn	0.50000	0.50000	0.44897	
c = 4.0110			O ₁	0.50000	0.50000	-0.05816	
	O ₂	0.00000	0.50000	0.48410			

3.2. Raman spectroscopy

Fig.3 shows Raman spectra of BSTSn ceramic recorded at room temperature. From Fig. 3, two transverse optical modes [A_1 (TO)] and a longitudinal optical mode [A_1 (LO)] were observed in the range of $100\text{-}300\text{ cm}^{-1}$. The detected bound at around 303 cm^{-1} is a distinctive particular of the tetragonal phase and it is attributed to a combined mode [B1, E (TO + LO)]. This Raman bound corresponds to the asymmetrical vibration mode of TiO_6 octahedral. The frequencies of about 516 and 724 cm^{-1} are assigned to two mixed modes, [A_1 , E(TO)] and [A_1 , E(LO)] produced by Ba-O bands [31]. These results indicate the presence of tetragonal distortion in BSTSn ceramic.

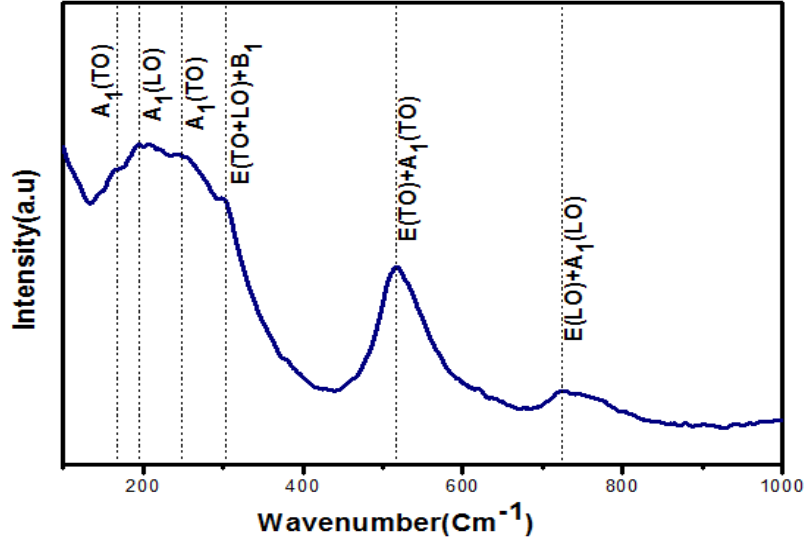


Fig. 3. Room temperature Raman spectra of BSTSn ceramic.

3.3. Microstructure analysis

Fig. 4 presents the SEM micrograph and grains morphology of BSTSn ceramic sintered at 1420°C/ 5h. The sample shows a dense microstructure with non-uniform grain size. The average grain size was determined using the Gaussian distribution of the grain and found to be around $6.80 \pm 0.17 \mu\text{m}$. Indeed, with sintering at such conditions, the BSTSn ceramic shows a pure, dense microstructure and small average grain size, which confirm the good quality of the ceramic for excellent electrical properties [32]. This result could be attributed to the fine crystallites obtained from the powder synthesized using sol-gel technic, as discussed in the X-ray diffraction section above. The fine particles obtained tend to agglomerate, resulting in a non-uniform and well-connected grain [33].

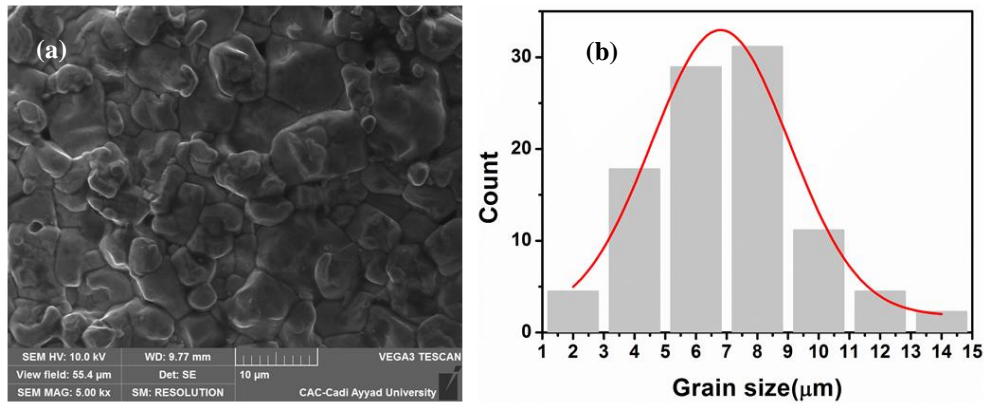


Fig. 4. (a) SEM micrograph and (b) grain size distribution of BSTSn ceramic sintered at 1420°C/5h.

3.4. Dielectric properties

Fig. 5 (a) and (b) show the temperature dependence of dielectric constant (ϵ_r) and dielectric loss ($\text{tg}\delta$) of BSTSn ceramic in the frequency range 100 Hz – 1 MHz. The ϵ_r increases with increasing temperature and reveals a maximum value (ϵ_m) of 5484 (1 kHz of frequency) at $T_c = 25^\circ\text{C}$, which corresponds to the temperature phase transition from ferroelectric to paraelectric phase. These results are in good agreement with those reported in the literature for BSTSn ceramics [26]. The obtained ϵ_m in this work is relatively low in comparison with those mentioned for BSTSn ceramics prepared by the conventionnel solid-state method, in which a high calcination temperature is adopted [23]. On the other hand, the relatively low value of $\epsilon_m \sim 5500$ could be attributed to the small grain size obtained for this composition by sol-gel method. One can see from Fig.5 (a) and (b), that both dielectric constant and dielectric loss are

decreasing with increasing frequency. This decrease could be attributed to the decrease of the contributions of different polarizations at high frequencies [34].

In the paraelectric region, the dielectric response usually follows the Curie-Weiss law for ($T > T_C$):

$$\frac{1}{\epsilon_r} = \frac{(T - T_0)}{C} \quad (2)$$

where T_0 and C are the Curie-Weiss temperature and the Curie-Weiss constant, respectively. Fig.5 (c) display the temperature evolution of the inverse dielectric constant ($\frac{1}{\epsilon_r}$) at 1 kHz of BSTSn ceramic. Good agreement between experimental data and those calculated by using Eq. (2) is observed. The calculated parameters are listed in Table 3. The obtained value of $C \sim 10^5$ K confirms the displacive-type ferroelectric of BSTSn ceramic.

To explain the diffuser behavior of the phase transition, the parameter ΔT_m is used to reveal the degree of diffuseness. This parameter was determined by using the following equation [35]:

$$\Delta T_m = T_{dev} - T_m \quad (3)$$

here, T_{dev} is the temperature at which the dielectric constant begins to deviate from the Curie-Weiss law and T_m is the temperature corresponding to the maximum dielectric constant.

The temperature dependence of the dielectric permittivity, above its maximum, has been extensively investigated as an important parameter to determine the character of phase transition in relaxor ferroelectrics. In this region, temperature-frequency dependence is not detected in ϵ_r versus T curves for the majority of relaxors [36]. The diffuseness coefficient of a diffuse phase transition (DPT) has been extracted from the Eq. (4) below known as the modified Curie-Weiss law:

$$\frac{1}{\epsilon_r} - \frac{1}{\epsilon_m} = \frac{(T - T_m)^\gamma}{C^*} \quad (4)$$

where γ is the constant that defines the transition diffuseness degree, C^* is the modified Curie-Weiss constant and T_m is the temperature corresponding to the ϵ_m . The characteristics of the phase transition depend on γ values. $\gamma = 1$ indicates the so-called ‘‘conventional’’ ferroelectric phase transition while when $\gamma = 2$, we have a ‘‘complete’’ DPT. Intermediate values of γ between 1 and 2 describe an ‘‘incomplete’’ DPT [37]. Fig. 5(d) presents the plot of $\ln(\frac{1}{\epsilon_r} - \frac{1}{\epsilon_m})$ versus $\ln(T - T_m)$ at a selected frequency of 1 kHz. The adjustable parameters are resumed in Table 3. The obtained γ value of BSTSn sample was found to be 1.62 indicating an incomplete diffuse phase transition.

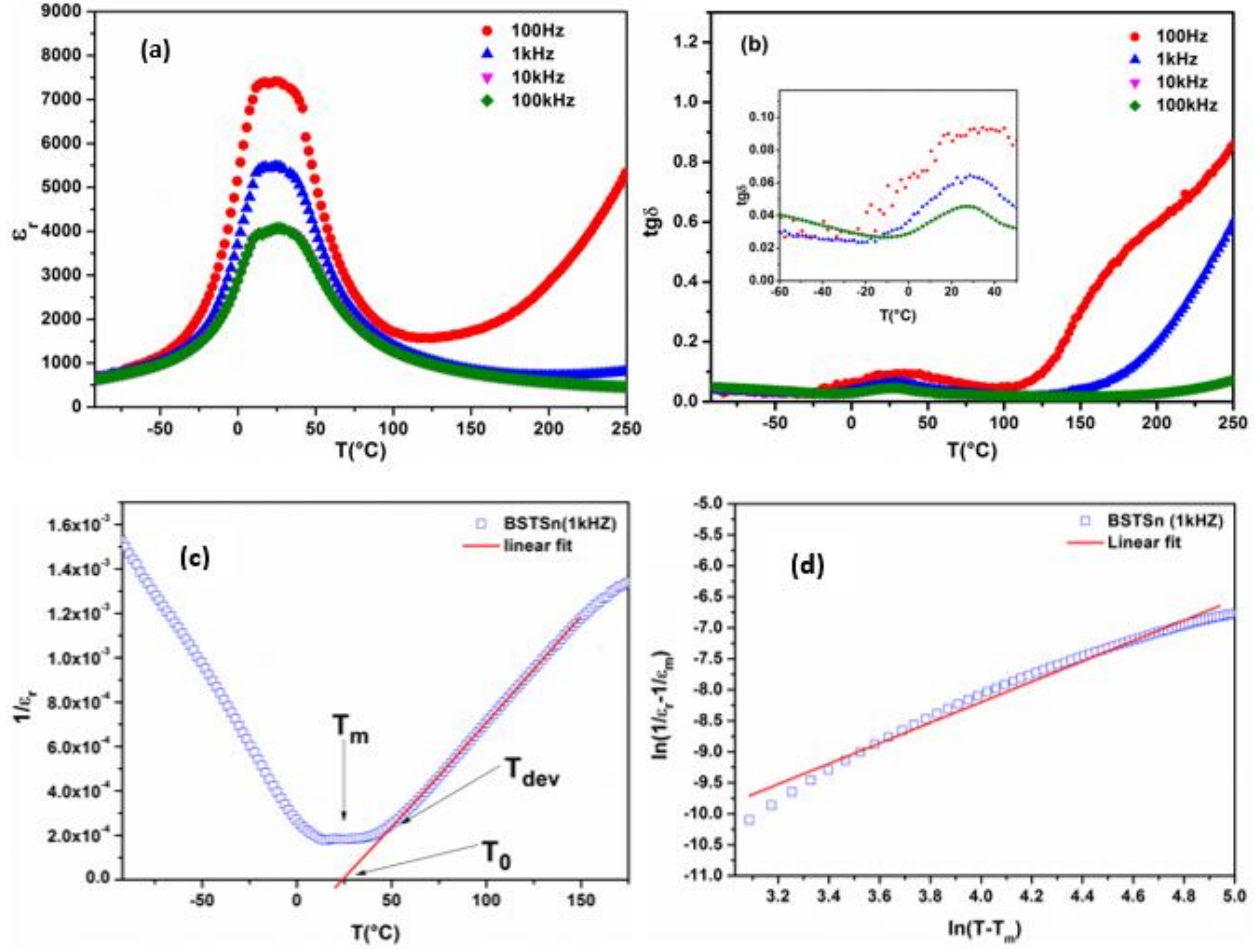


Fig.5 .(a) temperature- dependence of dielectric constant,(b) temperature- dependence of dielectric losses, (c) Thermal variation of $1/\epsilon_r$, and (d) showing plot of modified Curie-Weiss law at 1kHz of BSTS ceramic sintered at 1420°C/5h.

Table. 3 Adjustable parameters obtained from Eqs. (2), (3) and (4) of BSTSn ceramic at 1kHz.

	ϵ_m	$T_0(^{\circ}\text{C})$	$T_m(^{\circ}\text{C})$	$C \times 10^5$	T_{dev}	ΔT_m	γ
BSTSn	5484	26	23.6	1.04	52.81	29.21	1.62

3.5. Ferroelectric properties

In order to explore the ferroelectric properties of the BSTSn ceramic, the polarization-field ($P - E$) hysteresis loop was performed at RT and 200 Hz of frequency (Fig. 6). Typical ferroelectric $P - E$ cycle is observed which confirms the ferroelectric nature of BSTSn ceramic. Indeed, the studied sample presents a very narrow hysteresis cycle with a suitable symmetric shape. It is found that BSTSn sample show high spontaneous (P_s) polarization value of 11.44 $\mu\text{C}/\text{cm}^2$ with low values of remanent polarization (P_r) and coercive field (E_c) of 2.94 $\mu\text{C}/\text{cm}^2$ and 0.53 KV/cm, respectively under an applied field of 23 KV/cm. These findings indicate that BSTSn ceramics are very promising for energy storage applications. It is worth to mentioning that the maximum applied field of BSTSn in our study is very high than the one applied for BSTSn ceramics prepared by the solid-state method [23]. This result demonstrates that the sol-gel method is suitable for synthesizing ceramics with moderate breakdown strength.

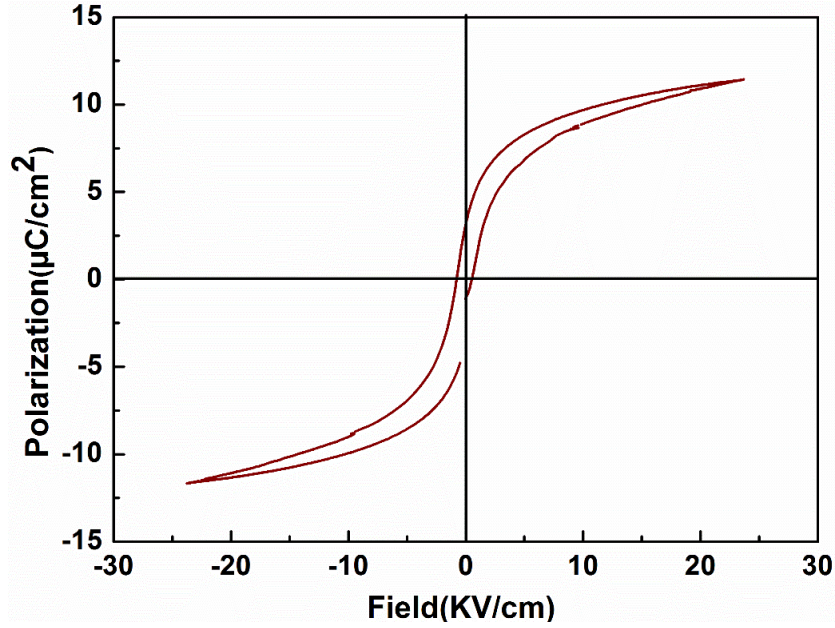


Fig. 6. Hysteresis loop of BSTSn ceramic obtained at room temperature.

3.6. Complex impedance analysis

In order to perform a thorough study of the electrical characteristics of BSTSn sample, the complex impedance spectroscopy (SIC) was used. Fig. 7 depicts the Nyquist plots ($-Z''$ versus Z') of BSTSn sample at different temperatures. The impedance spectrum from RT up to 300 °C is not shown in the figure (Fig. 7) as they just demonstrated a straight line with a large slope suggesting the insulating behavior of the sample. Nevertheless, while increasing temperature (far away from T_C), the semi-circular arcs are formed. In the present case, our experimental data are located on two semicircles, that can be attributed to the grain and grain boundaries contributions at high and lower frequencies, respectively [38]. Moreover, the radius of both semicircles was found to decrease with increasing temperature indicating the increase in conductivity of the sample with temperature. The complex impedance spectra was well fitted by using Z-View software with an equivalent electric circuit consisting of two parallel resistance and a constant phase element (R//CPE) connected in series (red fitted line). The resistances of both grain (R_G) and grain boundaries (R_{GB}) at different temperatures were extracted from fitting results and plotted in Fig. 8 as a function of the inverse of temperature. The activation energy process (E_a^R) of both R_G and R_{GB} was investigated. The evolution of both resistances obey to the Arrhenius law given by:

$$R = R_0 \exp\left(\frac{E_a^R}{k_B T}\right) \quad (5)$$

Where R_0 is the pre-exponential factor and k_B is the Boltzmann constant. It was reported in the literature that the oxygen vacancies can be easily created during the sintering process at high temperatures in perovskite materials containing titanate [39]. For perovskite oxides, the activation energy for conduction in the ranges of 0.3–0.5 eV and 0.6–1.2 eV have been associated to the singly and doubly ionized oxygen vacancies (V'_O , V''_O), respectively [40]. One can see from Fig. 8 that the evolution of both R_G and R_{GB} in the studied range temperature [300 – 380°C] can be separated into two regions ($T < 340^\circ\text{C}$) and ($T > 340^\circ\text{C}$). Therefore, two activation energies were deduced for each contribution. The activation energies were found to be 0.45 eV and 0.87 eV for both grains and grain boundaries, respectively for ($T < 340^\circ\text{C}$). These values of activation energy suggest that the conduction process below 340 °C is governed only by the oxygen vacancies singly and doubly ionized. However, for $T > 340^\circ\text{C}$, the activation energies were found to be higher than 2 eV for both contributions, which suggests that the conduction process could be assigned to the barium vacancies along with the oxygen vacancies [41].

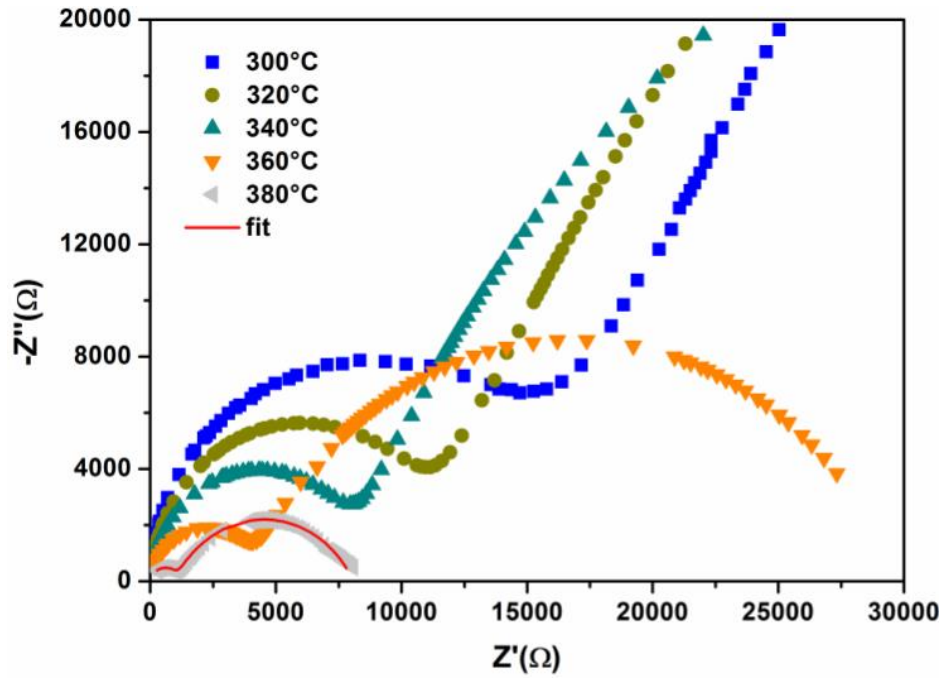


Fig. 7. Nyquist plot of BSTSn ceramic at various temperatures. The fitted curve is represented by a red line for representative temperature (380°C).

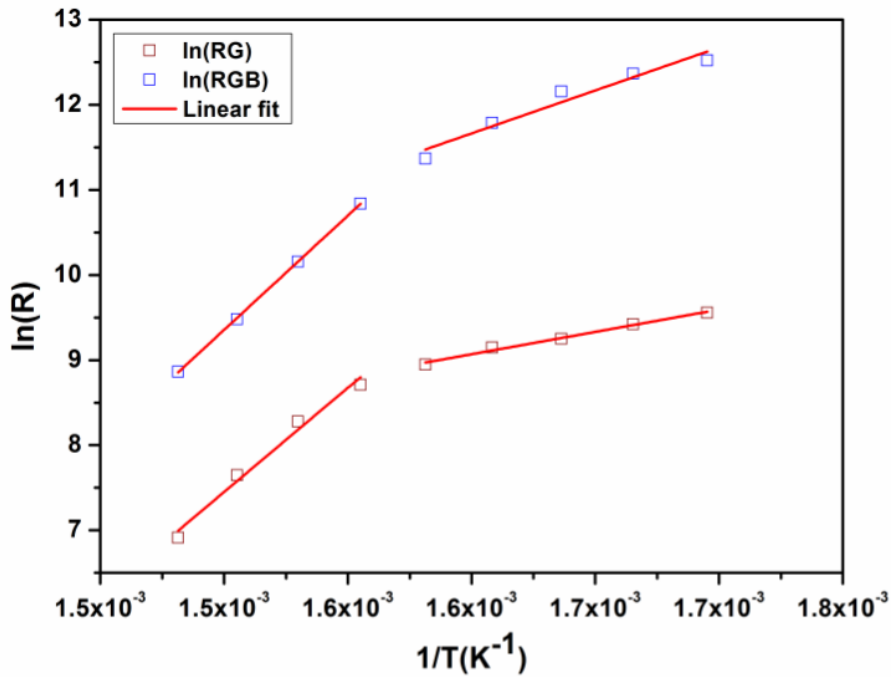


Fig. 8. Variation of the resistance of grain and grain boundaries as a function of the inverse of temperature for BSTSn ceramic.

4. Conclusion

In the present work, lead-free $\text{Ba}_{0.9}\text{Sr}_{0.1}\text{Ti}_{0.9}\text{Sn}_{0.1}\text{O}_3$ ceramic was successfully synthesized by the Sol-gel process. The XRD analysis showed a pure perovskite with a tetragonal structure refined in P4mm space group. The scanning

electron microscopy showed a relatively large grain size ($6.80 \pm 0.17 \mu\text{m}$) for BSTSn ceramic sintered at 1420°C . The dielectric analysis of BSTSn ceramic reveals a relatively high dielectric constant of ~ 5484 at room temperature with low dielectric losses less than 0.06. The modified Curie-Weiss law was used to study the diffuseness of BSTSn ceramic at 1kHz and suggests the incomplete diffuse nature of the transition. The ferroelectric nature of BSTSn ceramic was highlighted by P-E hysteresis loops and the values of the different parameters P_s , P_r and E_c were determined at RT. Different activation energies for conduction were observed in the temperature range $300 - 380^\circ\text{C}$. The obtained values reveal that the conduction mechanism in our BSTSn sample originated from the oxygen vacancies (singly and doubly ionized) below 340°C and barium vacancies above 340°C . Such properties make BSTSn ceramics a potential candidate for divers highly developed technological applications working at RT. For future research, the material selected in this study will be used as a target for synthesizing thin films by depletion laser technique.

Acknowledgments

The authors gratefully acknowledge the financial support of CNRST Priority Program PPR15/2015 and the European H2020-MSCA-RISE-2017-ENGIMA action.

References

- [1] W. J. Kim *et al.*, « Microwave properties of tetragonally distorted $(\text{Ba}_{0.5}\text{Sr}_{0.5})\text{TiO}_3$ thin films », *Appl. Phys. Lett.*, vol. 76, n° 9, p. 1185-1187, févr. 2000, doi: 10.1063/1.125977.
- [2] A. Ioachim *et al.*, « Barium strontium titanate-based perovskite materials for microwave applications », *Progress in Solid State Chemistry*, vol. 35, n° 2-4, p. 513-520, janv. 2007, doi: 10.1016/j.progsolidstchem.2007.01.017.
- [3] Y. Yao *et al.*, « Large piezoelectricity and dielectric permittivity in $\text{BaTiO}_3-x\text{BaSnO}_3$ system: The role of phase coexisting », *EPL*, vol. 98, n° 2, p. 27008, avr. 2012, doi: 10.1209/0295-5075/98/27008.
- [4] W.-C. Lee, C.-Y. Huang, L.-K. Tsao, et Y.-C. Wu, « Chemical composition and tolerance factor at the morphotropic phase boundary in $(\text{Bi}_{0.5}\text{Na}_{0.5})\text{TiO}_3$ -based piezoelectric ceramics », *Journal of the European Ceramic Society*, vol. 29, n° 8, p. 1443-1448, mai 2009, doi: 10.1016/j.jeurceramsoc.2008.08.028.
- [5] M. Cernea, E. Andronescu, R. Radu, F. Fochi, et C. Galassi, « Sol-gel synthesis and characterization of BaTiO_3 -doped $(\text{Bi}_{0.5}\text{Na}_{0.5})\text{TiO}_3$ piezoelectric ceramics », *Journal of Alloys and Compounds*, vol. 490, n° 1-2, p. 690-694, févr. 2010, doi: 10.1016/j.jallcom.2009.10.140.
- [6] L. Veselinović *et al.*, « The effect of Sn for Ti substitution on the average and local crystal structure of $\text{BaTi}_{1-x}\text{Sn}_x\text{O}_3$ ($0 \leq x \leq 0.20$) », *J Appl Crystallogr*, vol. 47, n° 3, p. 999 - 1007, juin 2014, doi: 10.1107/S1600576714007584.
- [7] C. Bhardwaj, B. S. S. Daniel, et D. Kaur, « Pulsed laser deposition and characterization of highly tunable $(1-x)\text{Ba}(\text{Zr}_{0.2}\text{Ti}_{0.8})\text{O}_3-x(\text{Ba}_{0.7}\text{Ca}_{0.3})\text{TiO}_3$ thin films grown on LaNiO_3/Si substrate », *Journal of Physics and Chemistry of Solids*, vol. 74, n° 1, p. 94-100, janv. 2013, doi: 10.1016/j.jpcs.2012.08.005.
- [8] P. Kumar et C. Prakash, « Enhanced electrocaloric effect in lead free $\text{Ba}_{0.90}\text{Sr}_{0.10}\text{Ti}_{1-3x/4}\text{Fe}_x\text{O}_3$ ceramics », *Journal of Alloys and Compounds*, vol. 839, p. 155461, oct. 2020, doi: 10.1016/j.jallcom.2020.155461.
- [9] X. Niu *et al.*, « Enhanced electrocaloric effect at room temperature in Mn^{2+} doped lead-free $(\text{BaSr})\text{TiO}_3$ ceramics via a direct measurement », *J Adv Ceram*, vol. 10, n° 3, p. 482-492, juin 2021, doi: 10.1007/s40145-020-0450-1.
- [10] S.-G. Lu *et al.*, « Enhanced electrocaloric strengths at room temperature in $(\text{Sr}_x\text{Ba}_{1-x})(\text{Sn}_{0.05}\text{Ti}_{0.95})\text{O}_3$ lead-free ceramics », *Journal of Alloys and Compounds*, vol. 871, p. 159519, août 2021, doi: 10.1016/j.jallcom.2021.159519.
- [11] Y. H. Huang, J. J. Wang, T. N. Yang, Y. J. Wu, X. M. Chen, et L. Q. Chen, « A thermodynamic potential, energy storage performances, and electrocaloric effects of $\text{Ba}_{1-x}\text{Sr}_x\text{TiO}_3$ single crystals », *Appl. Phys. Lett.*, vol. 112, n° 10, p. 102901, mars 2018, doi: 10.1063/1.5020515.
- [12] Z. Song *et al.*, « Thermal annealing effects on the energy storage properties of BST ceramics », *J Am Ceram Soc*, vol. 100, n° 8, p. 3550-3557, août 2017, doi: 10.1111/jace.14903.
- [13] C. Mao, X. Dong, T. Zeng, H. Chen, et F. Cao, « Nonhydrolytic sol-gel synthesis and dielectric properties of

- ultrafine-grained and homogenized Ba_{0.70}Sr_{0.30}TiO₃ », *Ceramics International*, vol. 34, n° 1, p. 45-49, janv. 2008, doi: 10.1016/j.ceramint.2006.08.002.
- [14] J.-G. Cheng, J. Tang, J.-H. Chu, et A.-J. Zhang, « Pyroelectric properties in sol-gel derived barium strontium titanate thin films using a highly diluted precursor solution », *Appl. Phys. Lett.*, vol. 77, n° 7, p. 1035, 2000, doi: 10.1063/1.1289038.
- [15] Y. J. Wu, Y. H. Huang, N. Wang, J. Li, M. S. Fu, et X. M. Chen, « Effects of phase constitution and microstructure on energy storage properties of barium strontium titanate ceramics », *Journal of the European Ceramic Society*, vol. 37, n° 5, p. 2099-2104, mai 2017, doi: 10.1016/j.jeurceramsoc.2016.12.052.
- [16] T. T. Chen, M. S. Fu, B. W. Jia, Y. J. Wu, X. Q. Liu, et X. M. Chen, « Dielectric and ferroelectric properties of Ba_{1-x}Sr_xTiO₃ ceramics: effects of grain size and ferroelectric domain », *Advances in Applied Ceramics*, vol. 112, n° 5, p. 270-276, juill. 2013, doi: 10.1179/1743676112Y.0000000070.
- [17] M. Arshad *et al.*, « Fabrication, structure, and frequency-dependent electrical and dielectric properties of Sr-doped BaTiO₃ ceramics », *Ceramics International*, vol. 46, n° 2, p. 2238 - 2246, févr. 2020, doi: 10.1016/j.ceramint.2019.09.208.
- [18] G. Dai *et al.*, « Direct and indirect measurement of large electrocaloric effect in barium strontium titanate ceramics », *Int J Appl Ceram Technol*, vol. 17, n° 3, p. 1354-1361, mai 2020, doi: 10.1111/ijac.13384.
- [19] N. Baskaran et H. Chang, « Effect of Sn doping on the phase transformation properties of ferroelectric BaTiO₃ », *J Mater Sci: Mater Electron*, vol. 12, p. 527-531, September 2001, doi: 10.1023/A:1012453526652.
- [20] W. Cai, Y. Fan, J. Gao, C. Fu, et X. Deng, « Microstructure, dielectric properties and diffuse phase transition of barium stannate titanate ceramics », *J Mater Sci: Mater Electron*, vol. 22, n° 3, p. 265-272, mars 2011, doi: 10.1007/s10854-010-0126-7.
- [21] M. Sanliarp *et al.*, « Direct measurement of electrocaloric effect in lead-free Ba(Sn_xTi_{1-x})O₃ ceramics », *Appl. Phys. Lett.*, vol. 111, n° 17, p. 173903, oct. 2017, doi: 10.1063/1.5001196.
- [22] S. Chihaoui, L. Seveyrat, V. Perrin, I. Kallel, L. Lebrun, et H. Khemakhem, « Structural evolution and electrical characteristics of Sn-doped Ba_{0.8}Sr_{0.2}TiO₃ ceramics », *Ceramics International*, vol. 43, n° 1, p. 427-432, janv. 2017, doi: 10.1016/j.ceramint.2016.09.176.
- [23] H. Zaitouni *et al.*, « Structural, dielectric, ferroelectric and tuning properties of Pb-free ferroelectric Ba_{0.9}Sr_{0.1}Ti_{1-x}Sn_xO₃ », *Ceramics International*, p. S0272884220322264, août 2020, doi: 10.1016/j.ceramint.2020.07.212.
- [24] L. Fu, L. Zhang, et X. Yao, « Structural and dielectric properties of Ba_{0.80}Sr_{0.20}Ti_{1-x}Sn_xO₃ ceramics », *J Electroceram*, vol. 21, n° 1-4, p. 561-564, déc. 2008, doi: 10.1007/s10832-008-9511-5.
- [25] R. Brahem, H. Rahmouni, N. Farhat, J. Dhahri, K. Khirouni, et L. C. Costa, « Electrical properties of Sn-doped Ba_{0.75}Sr_{0.25}Ti_{0.95}O₃ perovskite », *Ceramics International*, vol. 40, n° 7, p. 9355-9360, août 2014, doi: 10.1016/j.ceramint.2014.02.002.
- [26] H. Zaitouni *et al.*, « Direct electrocaloric, structural, dielectric, and electric properties of lead-free ferroelectric material Ba_{0.9}Sr_{0.1}Ti_{1-x}Sn_xO₃ synthesized by semi-wet method », *Physica B: Condensed Matter*, vol. 566, p. 55-62, août 2019, doi: 10.1016/j.physb.2019.04.026.
- [27] Y. Li, X. Yao, X. Wang, et L. Fu, « Tunability and Dielectric Properties of Ba_{1-x}Sr_xTi_{0.94}Sn_{0.06}O₃ Ceramics », *Ferroelectrics*, vol. 384, n° 1, p. 79-83, juin 2009, doi: 10.1080/00150190902892931.
- [28] H. L. Sun *et al.*, « Correlation of grain size, phase transition and piezoelectric properties in Ba_{0.85}Ca_{0.15}Ti_{0.90}Zr_{0.10}O₃ ceramics », *J Mater Sci: Mater Electron*, vol. 26, n° 7, p. 5270-5278, juill. 2015, doi: 10.1007/s10854-015-3063-7.
- [29] D. Segal, *Chemical Synthesis of Advanced Ceramic Materials*. Cambridge University Press, 1991.
- [30] R. Jacob, H. G. Nair, et J. Isac, « Structural and Morphological Studies of Nanocrystalline Ceramic BaSr_{0.9}Fe_{0.1}TiO₄ », *ILCPA*, vol. 41, p. 100-117, nov. 2014, doi: 10.18052/www.scipress.com/ILCPA.41.100.
- [31] U. D. Venkateswaran, V. M. Naik, et R. Naik, « High-pressure Raman studies of polycrystalline BaTiO₃ », *Phys. Rev. B*, vol. 58, n° 21, p. 14256-14260, déc. 1998, doi: 10.1103/PhysRevB.58.14256.
- [32] M. Chen *et al.*, « Polymorphic phase transition and enhanced piezoelectric properties in (Ba_{0.9}Ca_{0.1})(Ti_{1-x}Sn_x)O₃ lead-free ceramics », *Materials Letters*, vol. 97, p. 86 - 89, avr. 2013, doi: 10.1016/j.matlet.2012.12.067.
- [33] P.-Z. Ge, X.-G. Tang, Q.-X. Liu, Y.-P. Jiang, W.-H. Li, et J. Luo, « Energy storage properties and electrocaloric effect of Ba_{0.65}Sr_{0.35}TiO₃ ceramics near room temperature », *J Mater Sci: Mater Electron*, vol. 29, n° 2, p. 1075-1081, janv. 2018, doi: 10.1007/s10854-017-8008-x.
- [34] A. K. Singh, T. C. Goel, R. G. Mendiratta, O. P. Thakur, et C. Prakash, « Dielectric properties of Mn-substituted

- Ni–Zn ferrites », *J. Appl. Phys.*, vol. 91, n° 10, p. 6626, 2002, doi: 10.1063/1.1470256.
- [35] S. Hunpratub, S. Maensiri, et P. Chindaprasirt, « Synthesis and characterization of Ba_{0.85}Ca_{0.15}Ti_{0.9}Zr_{0.1}O₃ ceramics by hydrothermal method », *Ceramics International*, vol. 40, n° 8, p. 13025-13031, sept. 2014, doi: 10.1016/j.ceramint.2014.04.166.
- [36] I. A. Santos, D. Garcia, J. A. Eiras, et V. L. Arantes, « Features of diffuse phase transition in lead barium niobate ferroelectric ceramics », *Journal of Applied Physics*, vol. 93, n° 3, p. 1701 - 1706, févr. 2003, doi: 10.1063/1.1530366.
- [37] A. Belboukhari *et al.*, « Studies of Diffuse Phase Transition in Ferroelectric Solid Solution Pb_{1-x}K_{2x}Nb₂O₆ (x = 0.1, 0.2, 0.25 and 0.3) », *Ferroelectrics*, vol. 444, n° 1, p. 116 - 124, janv. 2013, doi: 10.1080/00150193.2013.786619.
- [38] T.-F. Zhang *et al.*, « Oxygen-vacancy-related relaxation and conduction behavior in (Pb_{1-x}Ba_x)(Zr_{0.95}Ti_{0.05})O₃ ceramics », *AIP Advances*, vol. 4, n° 10, p. 107141, oct. 2014, doi: 10.1063/1.4900610.
- [39] M. Sindhu, N. Ahlawat, S. Sanghi, R. Kumari, et A. Agarwal, « Effect of Zr substitution on phase transformation and dielectric properties of Ba_{0.9}Ca_{0.1}TiO₃ ceramics », *Journal of Applied Physics*, vol. 114, n° 16, p. 164106, oct. 2013, doi: 10.1063/1.4825123.
- [40] A. Peláiz-Barranco, « Dielectric relaxation and electrical conductivity in ferroelectric ceramic/polymer composites around the glass transition », *Appl. Phys. Lett.*, vol. 100, n° 21, p. 212903, mai 2012, doi: 10.1063/1.4720159.
- [41] B. K. Singh et B. Kumar, « Impedance analysis and high temperature conduction mechanism of flux grown Pb(Zn_{1/3}Nb_{2/3})_{0.91}Ti_{0.09}O₃ single crystal », *Cryst. Res. Technol.*, vol. 45, n° 10, p. 1003-1011, août 2010, doi: 10.1002/crat.201000287.